Osteoporos Int (1999) 9:339–345

Osteoporosis International

Original Article

Relationship Between Plain Radiographic Patterns and Three-dimensional Trabecular Architecture in The Human Calcaneus

G. Luo[1], J. H. Kinney[2], J. J. Kaufman[3], D. Haupt[2], A. Chiabrera[4] and R. S. Siffert[3]

[1]New York Department of Veterans Affairs Medical Center, New York, and Department of Rehabilitation Medicine, New York University Medical Center, New York, New York; [2]Department of Materials Science, Lawrence Livermore National Laboratories, Livermore, California; [3]Department of Orthopaedics, The Mount Sinai School of Medicine, New York, New York, USA; and [4]DIBE, University of Genoa, Genoa, Italy

Abstract. The purpose of this study was to determine the relationship between three-dimensional (3D) trabecular structure and two-dimensional plain radiographic patterns. An in vitro cylinder of human calcaneal trabecular bone was three-dimensionally imaged by micro-CT using synchrotron radiation, at 33.4 μm resolution. The original 3D image was processed using 14 distinct sequences of morphologic operations, i.e., of dilations and erosions, to obtain a total of 15 3D models or images of calcaneal trabecular bone. These 15 models had distinct densities (volume fractions) and architectures. The 3D structure of each calcaneal model was assessed using mean intercept length (fabric), by averaging individual fabric measurements associated with each medial-lateral image slice, and determining the relative anisotropy, R_{3D}, of the structure. A summated pattern or plain radiograph was also computed from the 3D image data for each calcaneal model. Each summated pattern was then locally thresholded, and the resulting two-dimensional (2D) binary image analyzed using the same fabric analysis as used for the 3D data. The anisotropy of the 2D summated pattern was denoted by $R_{x\text{-}ray}$. The volume fractions of the 15 models ranged from 0.08 to 0.19 with a mean of 0.14. The medial-lateral anisotropies, R_{3D}, ranged from 1.38 to 2.54 with a mean of 1.88. The anisotropy of the 2D summated patterns, $R_{x\text{-}ray}$, ranged from 1.35 to 2.18 with a mean of 1.71. The linear correlation of the 3D trabecular architecture, R_{3D}, with the radiographic trabecular architecture, $R_{x\text{-}ray}$, was 0.99 ($p<0.0001$). This study shows that the plain radiograph contains architectural information directly related to the underlying 3D structure. A well-controlled sequential reproducible plain radiograph may prove useful for monitoring changes in trabecular architecture in vivo and in identifying those individuals at increased risk of osteoporotic fracture.

Keywords: Micro-CT; Osteoporosis; Plain radiograph; Three-dimensional; Trabecular bone; Trabecular architecture

Correspondence and offprint requests to: Robert S. Siffert, MD, Department of Orthopaedics, Box 1188, The Mount Sinai School of Medicine, One Gustave L. Levy Place, New York, NY 10029, USA. Tel: +1 (212) 288 7900. Fax: +1 (212) 879 6742.

Introduction

The accurate clinical assessment of bone strength and fracture risk is important for management of bone loss diseases such as osteoporosis. Current techniques such as dual-energy X-ray absorptiometry (DXA) provide accurate estimates of bone mass but do not always provide reliable estimates of bone strength and fracture risk. One reason may be that trabecular architecture, which is not identified in mass measurements, can also be an important factor contributing to bone strength. For example, in an in vitro study it was demonstrated that bone density alone could account only for about 65% of the variation in bone strength, and that by incorporating both density and architecture the predictability could be improved to 90% [1].

Methods for measuring trabecular architecture directly include invasive methods such as iliac bone biopsy [2,3] and noninvasive imaging techniques. The noninvasive

methods include X-ray micro-computed tomography (micro-CT) [4,5] and high-resolution magnetic resonance imaging (MRI) [6]. Both the invasive and noninvasive methods described above are impractical for routine clinical management and screening for osteoporosis due to their high costs.

Plain radiographs have also been investigated as a more practical alternative for noninvasively assessing bone. Although bone density cannot be accurately measured using plain radiographs [7], many studies have reported on the determination of architecture-related measures from plain radiographs. For example, in one early study textural image features were shown to be affected during periods of disuse in plain radiographs of the calcaneus [8]. The features studied included fractal dimension, run length and co-occurrence measures. Subsequent investigations relating trabecular architecture to patterns in plain radiographs have also been reported. For example, it has been reported that fractal dimension can be measured from plain radiographs of the human calcaneus with a precision of better than 2.1% [9]. Other plain radiographic studies have been reported as well [10–12].

Although plain radiographs appear to offer the potential to assess trabecular structure noninvasively, there is at present virtually no understanding as to the relationship between three-dimensional (3D) architecture and the associated two-dimensional (2D) radiographic pattern. Thus the purpose of this study was to examine this relationship, and to determine the specific connection existing between the 3D and 2D representations.

Materials and Methods

Sample Preparation and Micro-CT Scanning

A single human calcaneus from which all soft tissue had previously been removed was obtained from a commercial supplier. A cylindrical core 1.42 cm in diameter was cut from the posterior portion of the calcaneus in the medial-lateral direction, using an electric drill corer. The cortical shells were then removed using a rotating disk cutter to produce a 10.3 mm long cylindrical sample of calcaneal trabecular bone (Fig. 1).

The specimen was three-dimensionally imaged with synchrotron radiation. The radiation was made monochromatic at 25 keV with two silicon single crystals whose faces were cut parallel to the (220) diffraction planes. Tomography was performed with the X-ray microtomography apparatus according to a protocol described in detail elsewhere [13]. Two-dimensional radiographs of the specimen were obtained at half-degree rotational increments, and the data were reconstructed into 3D images by a Fourier filtered backprojection method. Although the spatial resolution of the instrument is 2 μm, for the purposes of this experiment the data were reconstructed in cubic volume elements (voxels) that were 16.7 μm on edge. Even at this resolution the volumetric data set contained over 600 megabytes of information. This was further reduced for the purposes of this study by rebinning the data into 33.4 μm cubes, and finally the data globally thresholded to segment the structure into bone (pixel value = 1) and marrow (pixel value = 0), that is, a binary image.

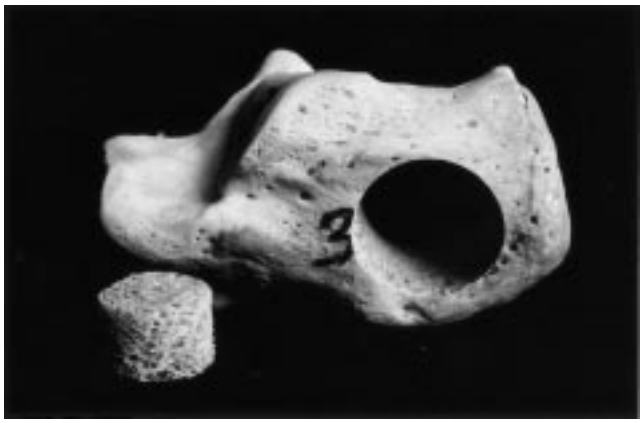

Fig. 1. Human calcaneus showing the trabecular core used in this study.

Digital Image Processing

Three-dimensional Data. The 3D image data corresponding to the single trabecular bone cylinder were then processed using sequences of morphologic image processing operations [14]. The original image data were eroded and dilated in 14 distinct sequences to obtain a total of 15 3D images (the original plus 14 transformed images). The distinct sequences of erosions and dilations were chosen arbitrarily, carried out in the medial-lateral direction, and used the classical erosion and dilation operators [15]. The 15 3D data sets were then analyzed for volume fraction and average fabric anisotropy. The fabric anisotropy of each of the 15 bone images was computed by averaging the fabric or mean intercept length (MIL) anisotropy feature of all the medial-lateral slices. In particular, the anisotropy feature of the 3D bone image, R_{3D}, was defined as the mean of the ratios of the MIL in the principal direction of the trabeculae to the MIL in the direction orthogonal to the principal direction, for all the slices in the 3D data set.

Summated Data. Each 3D data set was then summated along the medial-lateral direction in order to simulate a plain radiograph, shown schematically in Fig. 2. A planar image was produced according to the following relationship:

$$B(x,y) = 255\left[1 - \mathrm{e}^{-\mathrm{a}\sum_{z=1}^{N}\mu(x,y,z)}\right] \qquad (1)$$

where a is an arbitrary scale factor, $\mu(x,y,z)$ is an attenuation coefficient equal to 1 for solid (bone) phase

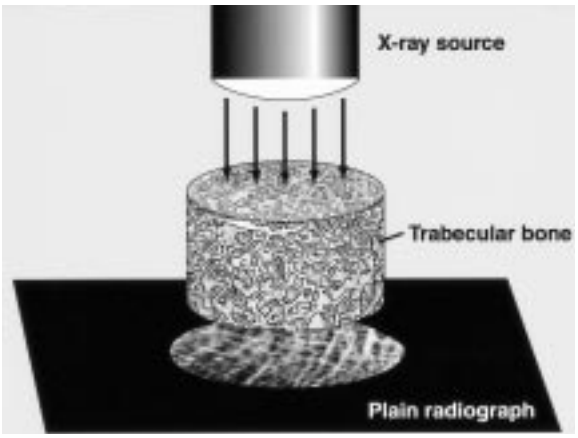

Fig. 2. Schematic representation of summated pattern generation from the 3D data sets.

and equal to 0 for void (marrow) phase, $N = 288$ is the total number of image slices, and $B(x,y)$ is the summated planar image. The 15 planar images, representing the summated patterns associated respectively with the 15 3D data sets and obtained according to Eq. 1 above, were then locally thresholded to obtain associated binary images. The local thresholding was carried out in order that a fabric MIL analysis could be performed. If $B(x,y)$ is assumed to be represented by an 8-bit pixel value, a threshold image, $T(x,y)$, was created using the following formula:

$$T(x,y) = \frac{\int_{y-\Delta/2}^{y+\Delta/2}\int_{x-\Delta/2}^{x+\Delta/2} B(\xi,\eta)\,d\xi\,d\eta}{\Delta^2} \qquad (2)$$

where Δ is the length of a side of a small square over which $T(x,y)$ is defined. After the creation of the threshold image, the locally thresholded image was defined as

$$B'(x,y) = \begin{cases} 255 & \text{if } B(x,y) \geq T(x,y) \\ 0 & \text{if } B(x,y) < T(x,y) \end{cases} \qquad (3)$$

where $B'(x,y)$ is the new binary image after local thresholding. In this study, the threshold length Δ was set equal to 0.67 mm (20 pixels). The fabric anisotropy, $R_{x\text{-ray}}$, of each of the 15 thresholded summated images was defined as the ratio of the MIL in the principal direction of the trabeculae to the MIL in the direction orthogonal to the principal direction, analogously as was done for the slices in the 3D images.

To address some of the more practical radiographic issues, noise was added to the ideal summated 2D radiographs (before thresholding) to gain some understanding of the sensitivity of the technique. In particular, uncorrelated Gaussian noise of zero mean and two different variances was added to each of the 15 simulated radiographs. The signal-to-noise ratio (SNR), in units of decibels (dB), was defined as

$$\text{SNR} = 20 \log_{10}\left[\frac{\max B(x,y)}{\sigma}\right] \qquad (4)$$

where σ (σ^2) was the standard deviation (variance) of the additive noise. For this study, σ = 5 and 10, respectively, leading to SNRs of 34 dB and 28 dB, respectively.

Results

A 3D rendering of the micro-CT data of the original calcaneal bone sample is shown in Fig. 3a. A single representative slice from the data set used to produce Fig. 3a is shown in Fig. 3b. Figure 3c shows the simulated plain radiograph associated with the original bone sample. Figure 4a–c show the analogous images as in Fig. 3a–c except that the 3D data set has undergone a series of two erosions, producing a structure of reduced volume fraction and increased anisotropy. Tables 1 and 2 provide a complete set of data used in this study and summary statistics, respectively. As may be seen, the volume fractions of the 15 data sets ranged from 0.08 to 0.19 with a mean of 0.14. The medial-lateral anisotropies ranged from 1.38 to 2.54 with a mean of 1.88. The anisotropy of the 2D summated patterns, $R_{x\text{-ray}}$, ranged from 1.35 to 2.18 with a mean of 1.71. Table 1 also indicates the specific sequence of dilations and/or erosions that were used to obtain the particular 3D image data.

The 3D trabecular architecture, R_{3D}, was then compared with the radiographic trabecular architecture, $R_{x\text{-ray}}$ (Fig. 5). The linear correlation of the 3D trabecular architecture, R_{3D}, with the radiographic trabecular pattern, $R_{x\text{-ray}}$, was 0.99 ($p<0.0001$). Table 3 shows the results of adding Gaussian noise to the ideal summated radiographs, for the two SNRs, as well as the noise-free images. As may be seen, the correlation between R_{3D} and $R_{x\text{-ray}}$, while somewhat reduced in the presence of noise, is still strongly significant, demonstrating a relative robustness of the overall fabric estimation procedure.

Discussion

Estimating fracture risk and bone strength in osteoporotic patients is an important clinical problem. Using bone mass alone is suboptimal but no other practical means currently exists for assessing bone integrity in vivo. Fabric is one measure of trabecular architecture, and has been shown, after mass, to be the most important feature related to bone strength. Whereas mass accounts for approximately 65% of the variation in observed bone strength, fabric can explain approximately an additonal 20–25% [1].

The results show that information on the average architecture fabric, i.e., mean intercept length, as measured in 3D samples, is contained in a summated

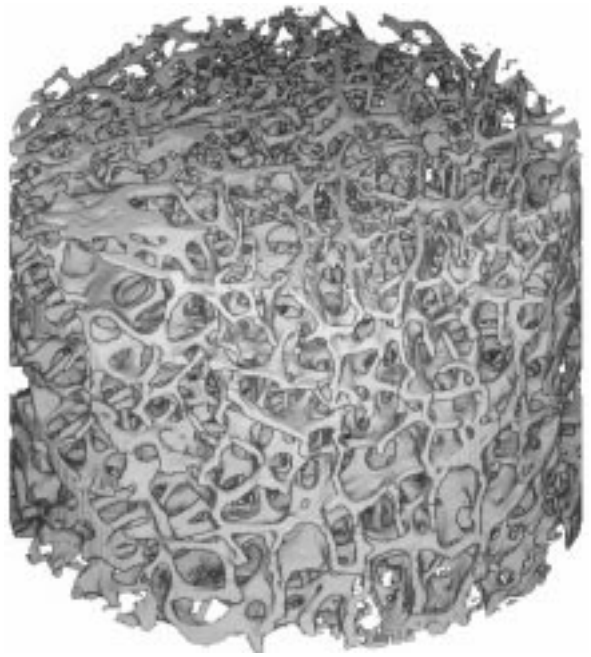

a

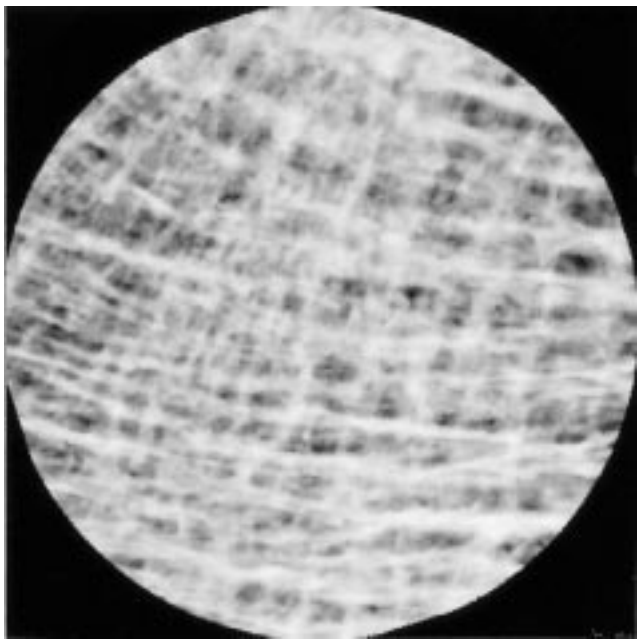

c

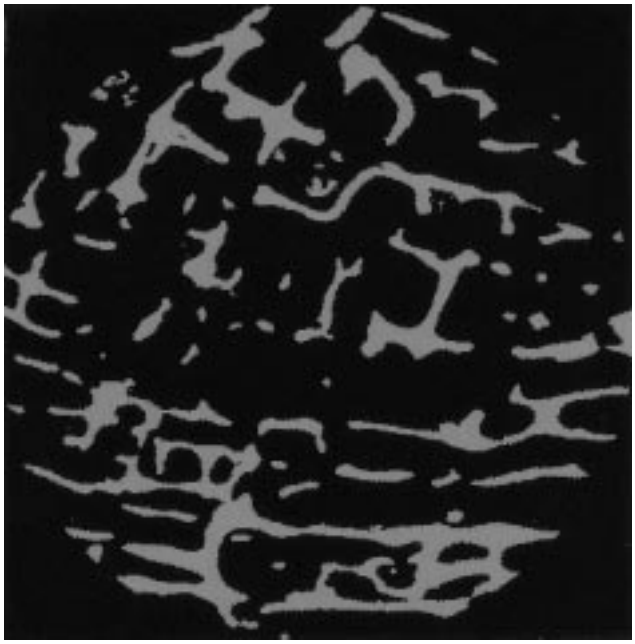

b

Fig. 3. a Three-dimensional rendering of the micro-CT data set of the original trabecular sample. **b** Representative single data slice from the image of **a**. **c** Summated gray-level pattern associated with the data of **a**.

2D image (i.e., a simulated plain radiograph). This is an important fact because it addresses a fundamental aspect of the X-ray process, namely summation, and shows that information on trabecular architecture is preserved in the transformation from 3D to 2D image. Though our study included only one bone sample, the use of the morphologic image processing operations produced data samples with a wide range of porosities and fabric architectures, in order to test our underlying hypotheses. Nevertheless, further studies with additional bone specimens, from different anatomic sites, are certainly warranted.

Although architectural (fabric) information is available in the 2D summated image, there are certain practical issues related to the X-ray processes and production of plain radiographs. To begin addressing this question, additive noise was introduced to the simulated radiographs. The results show that the techniques described for obtaining the fabric data from the 2D radiographs are quite robust with respect to the introduction of noise, showing only a 10% decrease in correlation value in going from no noise to 28 dB of SNR, for the linear regression of 2D versus 3D fabric measures. Such a SNR is typical of the systems described here [16]. This implies that the technique has reasonable characteristics with respect to reproducibility.

Additional practical considerations in the X-ray process that were not accounted for in this study (e.g.,

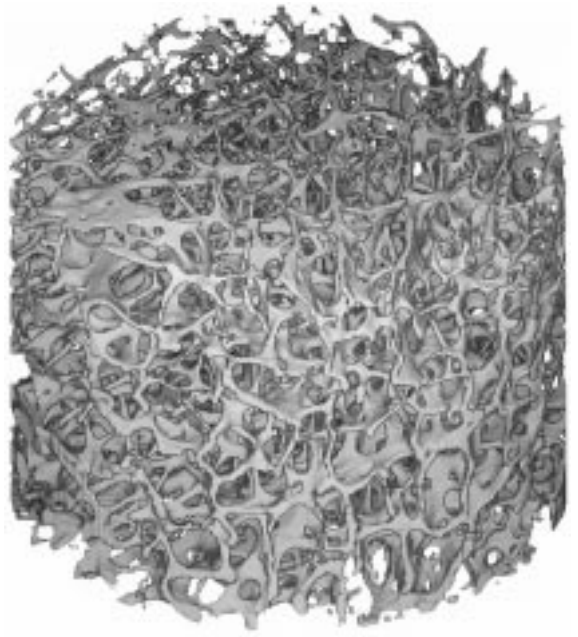

a

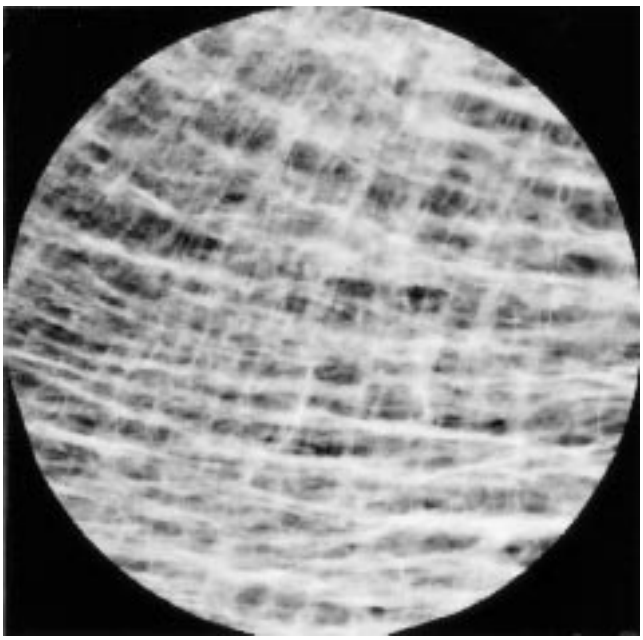

c

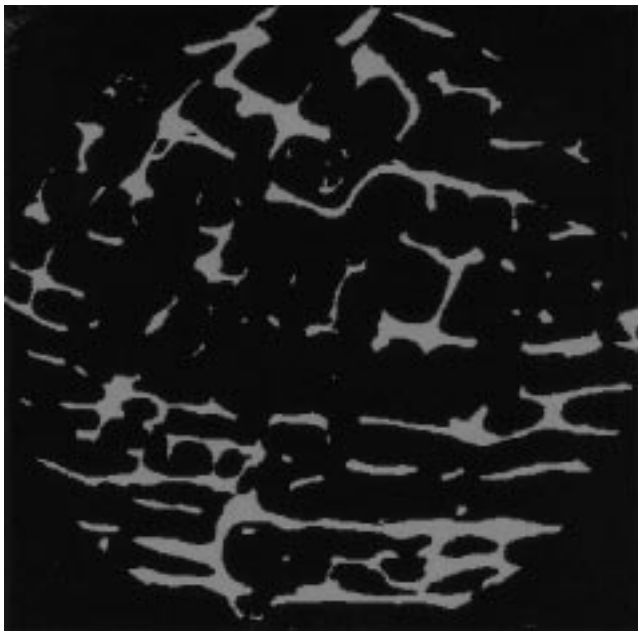

b

Fig. 4. a Three-dimensional rendering of the micro-CT data set after two erosions of the original trabecular sample. **b** Representative single data slice from the image of **a**. **c** Summated gray-level pattern associated with the data of **a**.

the monochromatic assumption and simplistic binary model used for the bone) place additional limitations on the generality of our findings. However, in a related but earlier pilot study [17] it has been shown using actual plain radiographs of human calcanei in vitro that fabric measured using methods identical to those described here is highly correlated with fabric as measured directly from a mid-sagittal trabecular bone slice. In addition, the actual radiographic images of the calcaneus are qualitatively similar to the simulated ones produced here. These observations suggest that the techniques described in the present study can be utilized in practical conditions and that artifacts associated with acquisition of film radiographs, including for example film processing, non-ideal exposure geometries and beams having a spread of photon energies, should not present excessive difficulties.

Although our study has focused on architectural fabric, as represented through measurements of the mean intercept length, other parameters of interest could also have been studied. For example, we have not addressed how the more classic histomorphometric parameters would transform from the original 3D sample onto the 2D radiographs [18,19], although that is certainly a question of some interest. We have focused on the use of architectural fabric since that is a parameter that has been specifically shown to be strongly related to bone elasticity and strength [1,20]. We also have not investigated the relationship of volume-based fabric parameters, such as volume orientation, with architecture

Table 1. Volume fraction and anisotropy data for the 15 images

	Volume fraction	R_{3D}	$R_{x\text{-}ray}$
Sample 1 (Original)	0.19	1.38	1.35
Sample 2 (E)	0.15	1.44	1.38
Sample 3 (EEEEDDD)	0.13	2.40	2.09
Sample 4 (EEE)	0.10	1.81	1.75
Sample 5 (EEDD)	0.18	1.70	1.54
Sample 6 (EEEE)	0.08	2.09	1.89
Sample 7 (EEEED)	0.10	2.12	1.90
Sample 8 (EEEEDD)	0.11	2.26	1.98
Sample 9 (EEEEDDDD)	0.14	2.54	2.18
Sample 10 (EED)	0.15	1.59	1.47
Sample 11 (EEED)	0.12	1.83	1.68
Sample 12 (EEEDD)	0.14	1.94	1.74
Sample 13 (EEEDDD)	0.16	2.07	1.85
Sample 14 (EE)	0.13	1.57	1.54
Sample 15 (ED)	0.18	1.49	1.38

Table 2. Summary statistics for the data in Table 1

	Volume fraction	R_{3D}	$R_{x\text{-}ray}$
Minimum	0.08	1.38	1.35
Maximum	0.19	2.54	2.18
Mean	0.137	1.88	1.71
Median	0.14	1.83	1.74
Standard deviation	0.0322	0.359	0.0687
95% confidence interval	0.0178	0.199	0.147

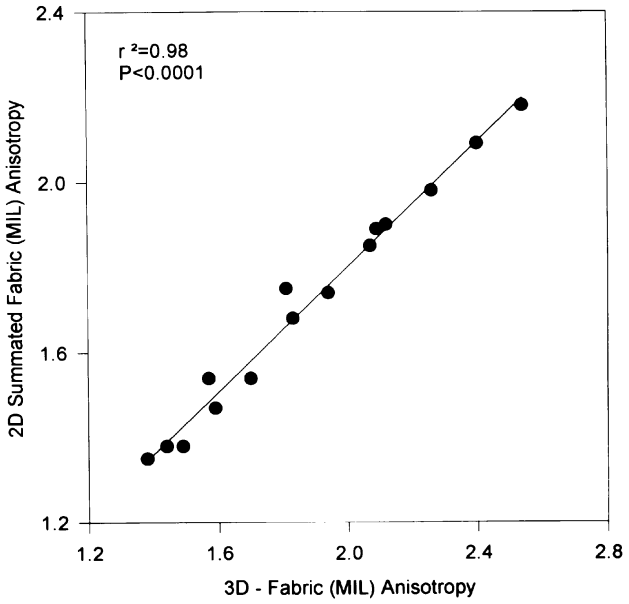

Fig. 5. Plot of 3D anisotropy versus summated pattern anisotropy, for the 15 data sets.

measured from the 2D radiograph, since it also has been shown that these volume-based measures perform only marginally better than fabric based on mean intercept length measurements [20,21]. Architecture, as measured by fabric, has also been shown in an adaptive remodeling simulation study to be related to bone elasticity, independently of bone mass [22].

Table 3. Effect of noise on correlations between R_{3D} and $R_{x\text{-}ray}$

	Correlation	*p*
No noise	0.99	<0.0001
SNR = 34 dB	0.95	<0.0001
SNR = 28 dB	0.89	<0.001

SNR, signal-to-noise ratio.

The importance of fabric architecture with respect to bone strength is somewhat contradicted by the insight that when bone is mechanically tested in a single well-controlled direction (e.g., vertebral trabecular bone uniformly tested only in the inferior-superior direction), then bone mass is an excellent predictor of elasticity and strength. It is typically when multiaxial loading is modeled (i.e., when bone is tested from a collection of directions) that fabric architecture leads to a significant improvement in bone strength estimation. How this translates into the clinical milieu is still a relatively open question, but it seems reasonable, based on the multi-axial nature of in vivo loading of bone, that fabric in particular and architecture in general can play a significant role in determining bone strength. A study using simulated multiaxial loading of trabecular bone samples that supports this viewpoint has been reported [22].

Further work is necessary to extend this work into clinical application. First, a standardized set of X-ray acquisition procedures needs to be developed. This should include development of automatic compensation techniques related to film development and exposure, as well as methods to obtain good reproducibility [16]. Previous studies on other radiographic feautres have demonstrated what appear to be adequate precisions [23,24] for clinical utility. Obtaining high relative precisions in estimations of architectural fabric from plain radiographs is an important aspect needed for further progress. Subsequently, clinical studies aimed at determining the utility of estimates of radiographic fabric will also need to be carried out. The overall purpose of such investigations will be to see whether radiographically determined fabric can improve a clinician's capability to estimate an individual's risk of osteoporotic fracture, over that obtainable by using bone mass measurements alone. In this regard, it is notable that a recent clinical study using high-resolution MRI of the calcaneus has demonstrated differences in trabecular structure between osteoporotic patients and controls [25]. Clearly, MRI is not an economically viable tool in terms of diagnosing and managing osteoporosis in the population at large. However, the fact that differences in trabecular structure in the calcaneus of osteoporotic versus normal individuals have been observed, when combined with the more theoretical results presented here, makes further investigations with plain radiographs warranted.

Acknowledgements. This work was supported in part by NIH grant #5T35DKO7420 and by private donor funds. The authors would also like to acknowledge the helpful discussions with Dr James T. Ryaby.

References

1. Turner CH, Rho JY, Ashman RB, Cowin SC. The dependence of elastic constants of cancellous bone upon structural density and fabric. Trans Orthopaed Res Soc 1998;13:74.
2. Cortet B, Colin D, Dubois P, Delcambre B, Marchandise X. Methods for quantitative analysis of trabecular bone structure. Rev Rhum Engl ed 1995;62:781–93.
3. Kaufman JJ, Einhorn TA, Klein M, Cowin S, Hatem M, Siffert RS. Iliac crest fabric measurements in osteoporotic patients. Trans Orthopaed Res Soc 1991;16:429.
4. Kinney JH, Lane NE, Haupt DL. In vivo, three-dimensional microscopy of trabecular bone. J Bone Miner Res 1995;10:264–70.
5. Muller R, Hildebrand T, Hauselmann HJ, Ruegsegger P. In vivo reproducibility of three-dimensional structural properties of non-invasive bone biopsies using 3D-pQCT. J Bone Miiner Res 1996;11:1745–50.
6. Chung HW, Wehrli FW, Williams JL, Kugelmass SD, Wehrli SL. Quantitative analysis of trabecular microstructure by 400 MHz nuclear magnetic resonance imaging. J Bone Miner Res 1995;10:803–11.
7. Genant HK, Engelke K, Fuerst T, Gluer C-C, Grampp S, Harris ST, et al. Noninvasive assessment of bone mineral and structure: state of the art [review]. J Bone Miner Res 1996;11:707–30.
8. Kaufman JJ, Mont MA, Hakim N, Ohley W, Lundahl T, Soifer T, Siffert RS. Texture analysis of radiographic trabecular patterns in disuse osteopenia. Trans Orthopaed Res Soc 1987;12:265.
9. Benhamou CL, Lespessailles E, Jacquet G, Harba R, Jeannane R, Loussot T, et al. Fractal organization of trabecular bone images on calcaneus radiographs. J Bone Miner Res 1994;9:1909–18.
10. Caliguri P, Giger ML, Favus MJ, Jia H, Doi K, Dixon LB. Computerized radiographic analysis of osteoporosis: preliminary evaluation. Radiology 1993;186:471–4.
11. Buckland-Wright JC, Lynch JA, Rymer J, Fogelman I. Fractal signature analysis of macroradiographs measures trabecular organization in lumbar vertebrae of postmenopausal women. Calcif Tissue Int 1994;54:106–12.
12. Siffert RS, Luo GM, Kaufman JJ. Moire patterns from plain radiographs of trabecular bone. In: Proceedings 17th Annual International Conference of the IEEE Engineering in Medicine and Biology Society. New York: IEEE, 1995.
13. Kinney JH, Nichold MC. X-ray tomographic microscopy using synchrotron radiation. Annu Rev Mater Sci 1992;22:121–52.
14. Serra J. Image analysis and mathematical morphology, vol 1. New York: Academic Press, 1982.
15. Russ JC. The image processing handbook, 2nd ed. Boca Raton, Florida: CRC Press, 1995.
16. Gonzalez RC, Wintz P. Digital image processing, 2nd ed. Reading, MA; Addison-Wesley, 1987.
17. Siffert RS, Luo GM, Kaufman JJ, Cowin SC. Quantitative analysis of trabecular architecture in plain radiographs of the human os calcis. In: Transactions of the 2nd Combined Meeting of the Orthopaedic Research Societies of USA, Japan, Canada and Europe. Palatine, IL: Orthopaedic Research Society, 1995.
18. Muller R, Van Campenhout H, Van Damme B, Van Der Perre G, Dequeker J, Hildebrand T, Ruegsegger P. Morphometric analysis of human bone biopsies: a quantitative structural comparison of histological sections and micro-computed tomography. Bone 1998;23:59–66.
19. Parfitt AM. Bone histomorphometry: proposed system for standardization of nomenclature, symbols, and units. Calcif Tissue Int 1988;42:284–6.
20. Van Reitbergen B, Odgaard A, Kabel J, Huiskes R. Relationships between bone morphology and bone elastic properties can be accurately quantified using high resolution computer reconstructions. J Orthop Res 1998;16:23–8.
21. Odgaard A, Kabel J, Van Reitbergen B, Dalstra M, Huiskes R. Fabric and elastic principal directions of cancellous bone are closely related. J. Biomech 1997;30:487–95.
22. Siffert RS, Luo GM, Cowin SC, Kaufman JJ. Dynamic relationships of trabecular bone density, architecture and strength in a computational model of osteopenia. Bone 1996;18:197–206.
23. Korstjens CM, Geraets WGM, Van Ginkel FC, Prahl-Andersen B, Van der Stelt PF, Burger EH. Longintudinal analysis of radiographic trabecular pattern by image processing. Bone 1995;17:527–32.
24. Geraets WGM, Van der Stelt, Netelenbos CJ, Elders PJM. A new method for automatic recognition of the radiographic trabecular pattern. J Bone Miner Res 1990;5:227–33.
25. Link TM, Majumdar S, Augat P, Lin JC, Newitt D, Lu Y, et al. In vivo high resolution MRI of the calcaneus: differences in trabecular structure in osteoporosis patients. J Bone Miner Res 1998;13:1175–82.

Received for publication 9 December 1997
Accepted in revised form 3 September 1998